Effect of graphene substrate type on formation of Bi $_2$ Se $_3$ nanoplates

(article starts on next page)

SCIENTIFIC REP˙RTS

OPEN

Effect of graphene substrate type on formation of Bi$_2$Se$_3$ nanoplates

Jana Andzane[1], Liga Britala[1], Edijs Kauranens[1], Aleksandrs Neciporenko[1], Margarita Baitimirova[1], Samuel Lara-Avila [2,3], Sergey Kubatkin[2], Mikhael Bechelany [4] & Donats Erts[1]

Knowledge of nucleation and further growth of Bi$_2$Se$_3$ nanoplates on different substrates is crucial for obtaining ultrathin nanostructures and films of this material by physical vapour deposition technique. In this work, Bi$_2$Se$_3$ nanoplates were deposited under the same experimental conditions on different types of graphene substrates (as-transferred and post-annealed chemical vapour deposition grown monolayer graphene, monolayer graphene grown on silicon carbide substrate). Dimensions of the nanoplates deposited on graphene substrates were compared with the dimensions of the nanoplates deposited on mechanically exfoliated mica and highly ordered pyrolytic graphite flakes used as reference substrates. The influence of different graphene substrates on nucleation and further lateral and vertical growth of the Bi$_2$Se$_3$ nanoplates is analysed. Possibility to obtain ultrathin Bi$_2$Se$_3$ thin films on these substrates is evaluated. Between the substrates considered in this work, graphene grown on silicon carbide is found to be the most promising substrate for obtaining of 1–5 nm thick Bi$_2$Se$_3$ films.

Recently, the integration of graphene with other Dirac materials (for example, topological insulator bismuth selenide (Bi$_2$Se$_3$)) has gained interest due to its potential to be used as a platform for the experimental realization of new room-temperature applications 2D TI structures[1,2]. For instance, these include thermoelectric devices[3] with Bi$_2$Se$_3$ being one of the best thermoelectric materials for near-room temperature applications. Other important applications are flexible composites for the use as anodes in lithium-ion batteries[4] and active elements in high-performance optoelectronic devices[5].

Bi$_2$Se$_3$ has rhombohedral crystal structure in the space group $R\bar{3}m$ with weak Van der Waals forces along the c-axis[6]. Each charge neutralized layer (quintuple layer, Q-layer) is formed by five covalently bonded atomic sheets (Se-Bi-Se-Bi-Se). Bi$_2$Se$_3$ can be deposited on solid substrates by variety of methods, including molecular beam epitaxy (MBE)[2,7], physical and chemical vapour deposition (PVD and CVD)[3,5,8], thermal evaporation[9].

Recent theoretical calculations performed for thermoelectrical properties of thin bismuth chalcogenide films predict that the reduction of the thickness of thin film below 10 nm may result in an increase of the existing thermoelectric figure of merit of this thin film by an order of magnitude[10]. Deep knowledge of Bi$_2$Se$_3$ nucleation and growth on various substrates is crucial for obtaining ultrathin continuous films of this material.

The PVD method remains one of the most promising to be used at industrial scale as it is simple, cost-effective and allows for large-scale production. However, unlike the highly controllable MBE method, growth of ultrathin Bi$_2$Se$_3$ nanostructures or continuous films by PVD deposition on different surfaces remains challenging. Hampering of lateral growth of the nuclei by physical and chemical defects of the substrate surface prevents layer-by-layer growth of Bi$_2$Se$_3$ films[11]. For obtaining of ultrathin nanostructures or films, atomically-flat, chemically-inert substrates are favourable.

Mica and graphene are recognized as excellent substrates for Bi$_2$Se$_3$ growth. Mica is chemically inert substrate with atomically flat surface ideal for Van der Waals epitaxy of Bi$_2$Se$_3$[1,12–16]. Despite a significant lattice mismatch between the mica and Bi$_2$Se$_3$ (~25%), the reported thicknesses for Bi$_2$Se$_3$ nanoplates deposited by PVD technique on synthetic fluorophlogopite mica surface are as small as 2–3 nm[15]. PVD synthesis on natural muscovite mica, which is cheaper alternative to synthetic mica, results in formation of Bi$_2$Se$_3$ nanoplates with thicknesses down to approx.10 nm. Continuous Bi$_2$Se$_3$ thin films grown on mica have thicknesses starting from 50 nm[12,16]. The thermoelectric power factor of these thin films is comparable with the Bi$_2$Se$_3$ thin films obtained by MBE

[1]Institute of Chemical Physics, University of Latvia, Riga, LV1586, Latvia. [2]Department of Microtechnology and Nanoscience, Chalmers University of Technology, SE-41296, Gothenburg, Sweden. [3]National Physical Laboratory, Hampton Road, Teddington, TW11 0LW, UK. [4]European Institute of Membranes, University of Montpellier, CNRS, ENSCM, 34095, Montpellier, France. Correspondence and requests for materials should be addressed to D.E. (email: donats.erts@lu.lv)
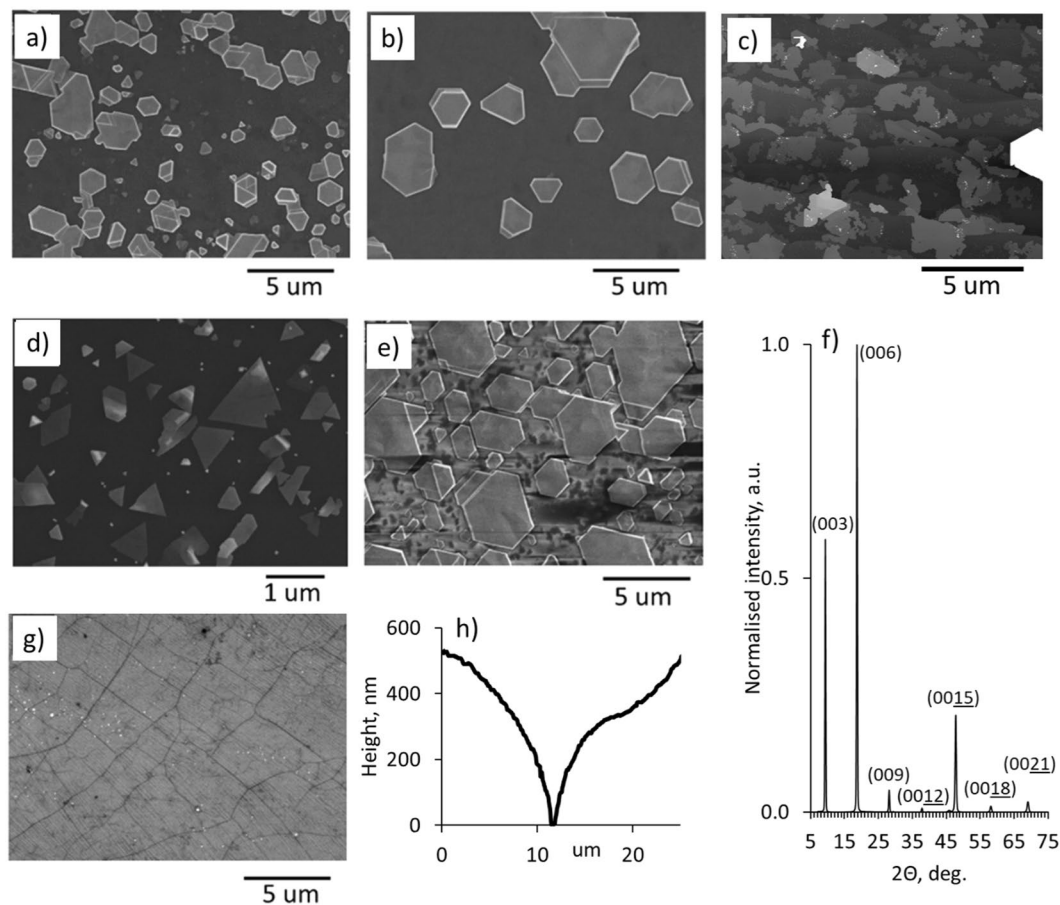
Figure 1. Scanning electron microscope (SEM) images of Bi_2Se_3 nanoplates deposited on the surface of (**a**) as-transferred CVD graphene; (**b**) post-annealed CVD graphene; (**c**) G/SiC substrate; (**d**) multilayer HOPG flake; (**e**) mica; (**f**) illustrative XRD pattern of a Bi_2Se_3 thin film formed from the nanoplates on the surface of as-transferred CVD graphene; (**g**) SEM image of CVD grown graphene transferred onto a glass substrate; (**h**) height profile of a typical grain boundary on the surface of copper substrate used for the CVD graphene synthesis.

techniques[12]. As for graphene, a very small lattice mismatch between graphene and Bi_2Se_3 (~2.9%)[1] makes it very attractive substrate to promote epitaxial growth of Bi_2Se_3 for the applications, where electrically conductive substrate is required.

Graphene substrates can be prepared by different methods, including CVD synthesis of graphene followed by its polymer-assisted transfer onto the desired substrate, mechanical exfoliation of highly ordered pyrolytic graphite (HOPG), thermal decomposition of SiC substrates (G/SiC), and others[17]. All these methods have advantages and drawbacks in terms of controllability, graphene quality, and costs. It is important to clarify how graphene substrates prepared by different techniques may differently affect the nucleation, further growth and properties of deposited on these substrates Bi_2Se_3.

This work is focused on a study of growth dynamics of Bi_2Se_3 nanoplates deposited by catalyst-free PVD technique on prepared by different methods (CVD followed by polymer-assisted transfer with and without post-annealing, SiC thermal decomposition) graphene substrates. The dimensions of deposited under the same experimental conditions onto graphene substrates nanoplates are compared with the dimensions of the Bi_2Se_3 nanoplates deposited on mica and exfoliated multilayer HOPG flakes used as reference substrates. Factors affecting nucleation and growth of the nanoplates are discussed, and the possibilities for further obtaining of ultrathin Bi_2Se_3 films on graphene substrates are evaluated.

Results and Discussion

Figure 1a–e show illustrative examples of Bi_2Se_3 nanoplates deposited on as-transferred and post-annealed CVD graphene, G/SiC, exfoliated multilayer HOPG flake and mica substrates.

Due to the intrinsically anisotropic bonding nature[18], normally the most energetically favourable orientation of Bi_2Se_3 nanoplates is with c-axis oriented perpendicularly (i.e. with Q-layers parallel to the surface of the substrate) to the commonly used for Bi_2Se_3 deposition substrates as graphene[3,5,7–9], SiO_2[11–13] and mica[14,15]. Diffraction peaks of XRD patterns obtained for the continuous Bi_2Se_3 thin films formed from the coalesced nanoplates on as-transferred CVD graphene surface (Fig. 1f) can be indexed to the rhombohedral structure with cell units of

Substrate	Thickness of Bi$_2$Se$_3$ nanoplates T, nm	Bi$_2$Se$_3$ nanoplates surface area S, um^2	Surface-to-thickness ratio S/T, x10^3 a.u.
CVD grapheme transferred on a glass substrate	50–375	0.4–11	2–60
Annealed CVD grapheme transferred on a glass substrate	30–360	0.4–30	2–170
Graphene on SiC substrate	1–20	1–50	30–2500
Exfoliated HOPG flake transferred on a glass substrate	18	1.13	63
	20	0.5	25
	21	1.85	88
	22	1.1	49
	22	1.4	63
	27	0.43	16
Natural mica (reference substrate)	6–240	0.3–20	11–240

Table 1. Dimensions of Bi$_2$Se$_3$ nanoplates deposited on different types of CVD graphene substrates, G/SiC, multilayer HOPG flake, and mica substrates.

a = b = 4.139 Å and c = 28.636 Å[19] (ref. code 00-033-0124), and are affiliated to a group (0 0 3n). This proves the growth of the Bi$_2$Se$_3$ layers in a single-crystalline phase with c-axis oriented perpendicularly to the substrate.

Generally, the top surfaces of the Bi$_2$Se$_3$ nanoplates are Se-passivated[20], resulting in much faster lateral growth of nanoplates than vertical due to diffusion of Bi and Se adatoms to the edges of the nanoplates. However, it is found in this study that the ranges of thicknesses and surface areas of the deposited under the same synthesis conditions nanoplates differ greatly for different graphene substrates. For relative comparison nanoplates dimensions, a parameter "surface-to-thickness ratio" (S/T) is used. For the S/T calculation, the surface area of the upper facet of a nanoplate is divided by the averaged thickness of this nanoplate. Both surface area and thickness are determined by the analysis of AFM scans of the nanoplates. The domination of the lateral growth direction over the vertical is indicated by higher values of S/T parameter. Data on the ranges of nanoplates thicknesses, surface areas and S/T ratios are summarised in Table 1 and comparative histograms in Figs 2 and 3f.
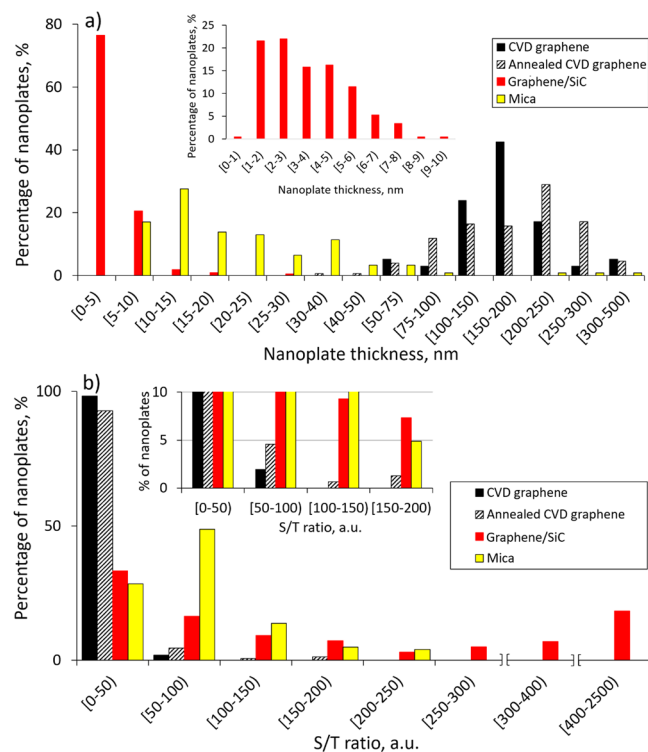
Thicknesses of the 75% of Bi$_2$Se$_3$ nanoplates deposited on mica (considered as a reference substrate) are below 25 nm, and 17% have thicknesses between 6 and 10 nm (Fig. 2a). It was expected that in contrast with mica, showing lattice mismatch with graphene of approx. 25%, a very small lattice mismatch of 2.9% between Bi$_2$Se$_3$ and a pure defect-less graphene will promote strain-free epitaxial 2D growth of crystalline Bi$_2$Se$_3$ layers[21,22]. At the initial stages of the Bi$_2$Se$_3$ deposition on graphene surface, such growth would result in formation of thin and large 2D islands of Bi$_2$Se$_3$ with higher S/T ratios than of the nanoplates deposited on mica.

As-transferred and post-annealed CVD graphene substrates.

Unexpectedly, the minimal thicknesses of the Bi$_2$Se$_3$ nanoplates deposited on CVD graphene exceed the minimal thicknesses of the Bi$_2$Se$_3$ nanoplates deposited on mica by 5–9 times (Fig. 2a). The thicknesses of the Bi$_2$Se$_3$ nanoplates deposited on as-transferred CVD graphene vary from 50 nm up to 375 nm (Table 1), with 9% of the nanoplates being below 100 nm thick (Fig. 2a). In turn, the thicknesses of the nanoplates deposited on post-annealed CVD graphene vary from 30 nm up to 360 nm with 17% of them being below 100 nm. This allows to conclude that post-annealing of the CVD graphene results in slight reduction of the nanoplates thicknesses in comparison with the nanoplates deposited on as-transferred CVD graphene. However, the post-annealing of transferred CVD graphene does not allow to reduce the thicknesses of the deposited nanoplates down to the dimensions comparable with the nanoplates deposited on mica substrate.

Even though the most thicknesses of the Bi$_2$Se$_3$ nanoplates deposited on as-transferred and post-annealed CVD graphene substrates fall in nearly the same range 50–300 nm (Table 1, Fig. 2a), the number of the nanoplates per unit area and lateral dimensions of the nanoplates deposited on these two types of substrates differ. The number of the nanoplates per unit area for as-transferred CVD graphene is higher, while their lateral dimensions are noticeably smaller in comparison with the nanoplates deposited on post-annealed CVD graphene (Fig. 1a,b, Table 1). As it can be seen from the histogram (Fig. 2b) and Table 1, the S/T parameters of the nanoplates deposited on mica cover the range from 11 to 240 with ~30% in the range [0–50), ~50% in the range [50–100) and ~19% in the range [100–200)). In contrast, 98% of the S/T parameters of the nanoplates deposited on as-transferred graphene are in the range [0–50) and the other 2% are in the range [50–100).

The nanoplates deposited on post-annealed graphene have higher than for as-transferred CVD graphene S/T values spread in the wider range (Figs 2b and 3f). These S/T values overlap with the S/T values of the nanoplates on mica in the range 11–170 (Table 1, Fig. 2b inset). However, the percentage of the nanoplates with higher S/T ratios grown on post-annealed is significantly smaller than for the nanoplates grown on mica. This indicate that the surface of post-annealed CVD graphene promotes lateral growth of the Bi$_2$Se$_3$ nanoplates better than the surface of as-transferred CVD graphene, but not good enough for formation of ultrathin Bi$_2$Se$_3$ films.

Presumably, the thicknesses and number per unit area of the Bi$_2$Se$_3$ nanoplates are defined by the number of surface defects of CVD graphene. One of the main causes of the surface defects of CVD graphene is its domain structure, arising from the grainy structure of copper substrate used during the CVD deposition[23]. Figure 1g,h illustrate respectively scanning electron microscope (SEM) image of a CVD graphene and a height profile of a typical grain boundary on the surface of copper foil used for CVD graphene deposition. Since the edges of the

Figure 2. Comparative histograms: (**a**) of the thicknesses of Bi_2Se_3 nanoplates, deposited on different graphene and mica substrates. Inset – histogram of the thicknesses of Bi_2Se_3 islands deposited on G/SiC substrates for the thickness range 1–10 nm; (**b**) of the S/T parameter of Bi_2Se_3 nanoplates, deposited on different graphene substrates and mica. Inset – closer look at the spread of the S/T parameter of the deposited on different substrates Bi_2Se_3 nanoplates.
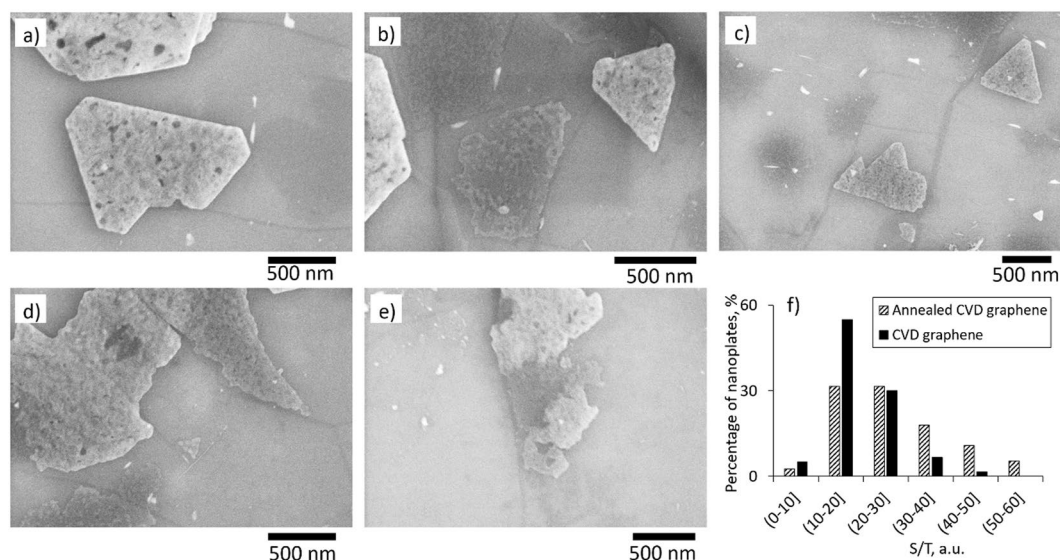
Figure 3. (**a–e**) SEM images of the initial stages of Bi_2Se_3 nanoplates formation on CVD graphene surface; (**f**) comparative histogram of the S/T ratios of the initial formation stage of the nanoplates on as-transferred and post-annealed CVD graphene.

copper domains are concave, it is possible that the graphene domains do not grow together completely. When transferring CVD graphene from the copper substrate, the domains may be joined mechanically. This may result in a large number of defects, creating potential barriers of 0.02–0.1V[13,24], as well as in some number of dangling bonds alone the domain boundaries. Presumably, such domain boundaries may serve as obstacles for the nanoplates lateral growth, and at the same time as nucleation centres. The role of graphene domain boundaries in

the formation of Bi$_2$Se$_3$ nanoplates is illustrated by the Fig. 3a–e, showing the initial stages of the nanoplates formation, occurring at high substrate temperatures (see the Methods section). The graphene domain boundaries interrupt symmetrical lateral growth of the nanoplates (for example see Fig. 3a), but at the same time may serve as nucleation centres (for example see Fig. 3d). The rugged surfaces of the nanoplates are due to the excess of Bi at the initial stages of the deposition, which is compensated during the later stages of the deposition occurring during the cooldown process (see the Methods section).

In addition to the impurities introduced by the domain boundaries, the CVD graphene may have significant number chemical surface defects formed during the transfer process[25]. For instance, it may be residual contamination with polymers used for the transfer. These defects also may serve as nucleation centres or lateral growth limiting factors for the nanoplates. Nucleation occurring on these defects together with hampering of the lateral growth of the nanoplates without affecting the speed of their vertical growth results in relatively high thicknesses of the nanoplates and their dense location. That means that the thin films grown on as-transferred CVD graphene will consist of higher number of grown together nanoplates per unit area in comparison with thin films grown on post-annealed CVD graphene. As the boundaries between the grains of nanostructures forming thin films are known to affect their electrical[26] and thermal[27] properties, the thermoelectric properties of the Bi$_2$Se$_3$ thin films deposited on as-transferred and post-annealed CVD graphene may differ.

Post-annealing of as-transferred CVD graphene leads to the partial healing of the chemical surface defects on the graphene surface[28] and elimination of the polymer residues[29,30]. This reduces the number of possible nucleation centres that may also hamper the nanoplates lateral growth on the graphene surface. This results in an increase of lateral dimensions of the nanoplates and decrease of their location density. However, post-annealing does not completely remove the obstacles for Bi$_2$Se$_3$ nanoplates lateral growth on the CVD graphene surface, as the minimal thickness of the nanoplates decreases insignificantly (30 nm, Table 1) and does not achieve the average thickness of the Bi$_2$Se$_3$ nanoplates deposited on mica (~22 nm with minimal thicknesses of 6 nm). Most probably, this effect can be attributed to the influence of the large domain boundaries, formed during the graphene growth on the copper substrates and remaining on the CVD graphene surface after its post-annealing. It should be noted that the nanoplates with thicknesses below 10 nm and large S/T parameters are crucial for formation of ultrathin continuous Bi$_2$Se$_3$ thin films. The conclusion is that both as-transferred and post-annealed CVD graphene substrates may be useful for obtaining of thick (~150–300 nm) nanostructured Bi$_2$Se$_3$ films. For obtaining of ultrathin Bi$_2$Se$_3$ films, alternative to CVD graphene substrates as, for instance, G/SiC should be considered.

Graphene/SiC and exfoliated HOPG flakes.

Using of G/SiC substrates allows to avoid the influence of such surface defects as domain boundaries or transfer-caused defects (polymer residues etc), increasing the number of nucleation centres and hampering the lateral growth of the Bi$_2$Se$_3$ nanoplates.

Thicknesses of the 75% of Bi$_2$Se$_3$ islands formed on the surface of G/SiC are found to be below 5 nm (Table 1, Fig. 2a). Thicknesses of nearly half (43%) of the Bi$_2$Se$_3$ islands are having thicknesses 3 nm and below (Fig. 2a inset). At average, thicknesses of the Bi$_2$Se$_3$ islands deposited on G/SiC substrates are ~5, 10 and 15 times smaller than the minimal thicknesses of the Bi$_2$Se$_3$ nanoplates deposited on as-transferred CVD graphene, post-annealed CVD graphene and mica substrates respectively.

It is observed that Bi$_2$Se$_3$ nucleation starts at the jagged edges of G/SiC terraces formed during the thermal decomposition of the SiC substrate (Fig. 4a). The lateral growth of Bi$_2$Se$_3$ 2D islands seems to be limited by the edges of the terraces similarly to the previously reported MBE deposition of Bi$_2$Se$_3$ on G/SiC substrates[7].

Presumably, the terraces formed on the G/SiC substrates are the main factor influencing Bi$_2$Se$_3$ nucleation and lateral growth due to the presence of the double-layer graphene areas along their edges. As it was reported in[31,32], this double-layer graphene exhibits higher surface energy in comparison with the single-layer graphene. Possibly, the Bi$_2$Se$_3$ nucleation may start at the promoting deposition areas of double-layer graphene and continue epitaxially.

In contrast with the S/T parameters of Bi$_2$Se$_3$ nanoplates deposited on as-transferred CVD graphene (96% of S/T is below 30) and post-annealed CVD graphene (81% of S/T is below 30), the S/T parameters for the Bi$_2$Se$_3$ islands formed on the G/SiC substrates are starting from 30 and are spread up to 2500 (Table 1, Fig. 2b). For the comparison, the amount of the deposited-on mica Bi$_2$Se$_3$ nanoplates with S/T below 30 is just about 7%. Thus, the S/T parameters for the Bi$_2$Se$_3$ islands deposited on G/SiC cover almost all the values of the S/T parameters for the nanoplates deposited on mica and expand up to the significantly (up to an order of magnitude) higher S/T values. 45% of the Bi$_2$Se$_3$ islands on G/SiC substrates are having higher S/T parameters than the largest S/T of mica-supported nanoplates (Fig. 2b). The high S/T ratios at small average thickness of the nanostructures are vital for formation of ultrathin films. This means that between the useful for practical application graphene substrates, the epitaxial graphene grown on SiC surface is the best substrate for 2D growth of Bi$_2$Se$_3$. In perspective, G/SiC substrates could be used for obtaining of ultrathin Bi$_2$Se$_3$ thin films with thicknesses 1–5 Q-layers. Also, separate Bi$_2$Se$_3$ nanoplates with large (up to 50 um^2) surface areas, thicknesses up to 20 nm (Table 1) and smooth graphene/Bi$_2$Se$_3$ interface can be formed on these substrates.

For the comparison with G/SiC substrates and illustration of the role of terraces in formation of Bi$_2$Se$_3$ nanoplates, the exfoliated multilayer HOPG flakes are used. As it is well known, graphene obtained by mechanical exfoliation of HOPG is of the best quality. However, the number of graphene layers in an exfoliated flake is difficult to control. Also, the HOPG flakes have terraced structure formed during the mechanical exfoliation. Average thickness of the nanoplates obtained on the flakes of exfoliated HOPG is ~21 nm with S/T ratios 18–88 (Table 1). These parameters are comparable with the parameters of the Bi$_2$Se$_3$ nanoplates deposited on mica. Characteristic for the Bi$_2$Se$_3$ triangular shapes of the separate nanoplates (Fig. 1d) indicate similar to mica absence of minor surface defects of this type of substrate. However, the Bi$_2$Se$_3$ nanostructures deposited on the HOPG flake surface are lined up, presumably along the graphite terrace edges. Such lining-up is clearly seen in the areas of the HOPG flake with more dense location of the Bi$_2$Se$_3$ nanoplates (Fig. 4b). This allows to conclude that in the case of HOPG
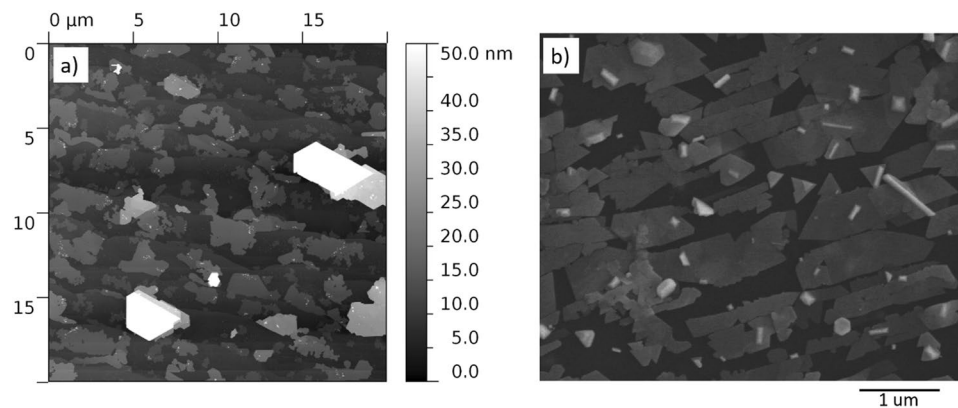
Figure 4. (**a**) Bi_2Se_3 islands formed on G/SiC substrate; (**b**) SEM images of the Bi_2Se_3 nanoplates formed on an exfoliated HOPG flake.

flake the growth mechanism is partly similar to this on the G/SiC substrate. The nucleation of the nanoplates starts at the edges of the terraces and expands epitaxially along the terrace surface. The higher average thickness of the nanoplates deposited on the exfoliated HOPG flake in comparison with the average thickness of the nanoplates deposited on G/SiC may possibly be explained by the specific features of G/SiC substrates as the presence of double-layer graphene with higher surface energy along the edges of the terraces and strain-less surface of the graphene, effectively promoting nucleation and epitaxial growth of the Bi_2Se_3.

Summary

Nucleation and further growth of Bi_2Se_3 nanoplates deposited by catalyst-free PVD method under the same experimental conditions on prepared by different methods graphene substrates is studied. The dimensions of these nanoplates are analysed and compared with the dimensions of Bi_2Se_3 nanoplates deposited on mechanically exfoliated natural mica and multilayer HOPG flake as reference substrates.

Following the analysis of the nanoplates dimensions in relation to specific features of the substrate, it can be concluded that the lateral growth of the nanoplates on as-transferred CVD graphene may be slowed down by the potential barriers of its domain boundaries, as well as by the other surface defects arising from the CVD graphene growth and transfer process. Hampering of the lateral growth of the nanoplates while vertical growth rate remains the same results in minimal thicknesses of the Bi_2Se_3 nanoplates of 50 nm.

Post-annealing of the CVD graphene eliminates the polymer contamination and heals minor graphene surface defects but is not affecting the graphene domain boundaries. Elimination of minor defects of the CVD graphene surface results in reduction of minimal thicknesses of the deposited nanoplates down to 30 nm and an increase of their S/T parameters in comparison with the as-transferred CVD graphene. Thin films grown on as-transferred CVD graphene are expected to have higher number of the nanoplates per unit area in comparison with thin films grown on post-annealed graphene. The difference in the number of the nanoplates per unit area may affect the electrical and thermal properties of the Bi_2Se_3 thin films grown on as-transferred and post-annealed CVD graphene substrates.

Graphene grown directly on the SiC substrate by its thermal decomposition method is found to be a very good substrate for 2D growth of Bi_2Se_3. The Bi_2Se_3 nucleation starts at the edges of the terraces of G/SiC substrate (presumably covered with double-layer graphene) and continues epitaxially. Lateral growth of Bi_2Se_3 islands is limited by the edges of the terraces. Similar growth mechanism is observed on the mechanically exfoliated multilayer HOPG flakes, where the deposited Bi_2Se_3 nanoplates were lined-up along the graphite terraces. However, the average thickness of the nanoplates deposited on HOPG flakes (~21 nm) is by at least 5 times larger than the average thickness of the nanoplates deposited on G/SiC (~4 nm). Possibly, this may be explained by specific issues of the G/SiC substrates as double-layer graphene with higher surface energy along the edges of the terraces and strain-less graphene surface. Thus, the G/SiC substrates are found to be the most perspective for obtaining of Bi_2Se_3 thin films with thicknesses below 5 nm. However, the drawback of using the G/SiC substrates is limitation by the wafer sizes (currently 6" available) and costs.

Methods

Bi_2Se_3 nanoplates synthesis. Bi_2Se_3 nanostructures were synthesized by modified catalyst-free vapour-solid deposition method reported elsewhere[3,33–35] using a quartz tube furnace (GCL-1100X, MTI Corp). The source material (Bi_2Se_3, 99.999%, Sigma Aldrich) was placed in a quartz boat in the centre of the furnace tube, while the substrate was located downstream relative to the source material.

For the synthesis, the furnace tube was flushed with N_2, pumped down to the base pressure 5 Torr and sealed. The centre of the quartz tube was heated at a rate of 13 °C/min to 585 °C. The substrate temperature for Bi_2Se_3 deposition was 410–450 °C. The temperature was held constant (at 585 °C) for 15 minutes for the initial formation of the nanoplates. Than the furnace was naturally cooled down to 465 °C. During this cooling process, the further growth of the nanoplates together with their enrichment with Se occurs. At furnace temperature of 465 °C, the furnace tube was filled with N_2 to atmospheric pressure, sealed and cooled down to room temperature. For the

study of the initial formation stages of the nanoplates, the substrate was taken out from the furnace tube at 585 °C and rapidly cooled down under the N_2 gas flow.

Substrate preparation. Glass substrates were washed in 2-propanol and distilled water, followed by drying under N_2 flow. Muscovite mica sheets (Agar Scientific) were mechanically cleaved immediately before the synthesis process.

As-transferred CVD graphene. Monolayer graphene was prepared by chemical vapour deposition method on copper foil and transferred on the quartz/glass substrates using polymer-assisted technique described elsewhere[20].

Annealing of CVD graphene. Glass substrates with transferred by polymer-assisted technique graphene was annealed consequently in air (250 °C, ambient pressure, 60 min) and H_2/Ar flow (0.2/0.4 L/min, 250 °C, base pressure 0.5 Torr, 60 mins).

Exfoliation of HOPG. HOP graphite flakes were mechanically exfoliated from the macro piece of HOPG and transferred onto the pre-cleaned glass substrate using adhesive tape (3M™ 8805).

G/SiC substrates. Monolayer graphene was grown on the Si-face of SiC using thermal decomposition of 7×7 mm SiC substrates (Cree, Inc). The 3" SiC wafer is diced into 7×7 mm chips, which are cleaned using solvents (acetone, isopropyl alcohol) and blow-dried with N_2. Chips are then cleaned using RCA 1 and 2 processes and dipped in HF (3%) for 30 seconds. The samples are loaded in a reactor for epitaxial graphene growth equipped with an inductive heater. Graphene growth takes place in argon atmosphere (P = 600 Torr) at a temperature of 1700 °C for 5 min. After growth, optical microscopy reveals a typical surface coverage of >90% monolayer graphene.

Investigation methods. Morphology, thickness, structure and composition of obtained Bi_2Se_3 nanostructures and nanostructured layers were inspected using field emission scanning electron microscope (SEM) Hitachi S-4800 equipped with an energy-dispersive X-ray (EDX) analyser Bruker XFLASH 5010 and atomic force microscopes Asylum Research MFP-3D and Bruker Dimension ICON.

For the statistical analysis, 5 to 9 AFM scans of size $20 \times 20\,\mu m$ each were obtained at different locations on the sample. The number of measured nanoplates was 110–150 for each type of the substrate with an exclusion of exfoliated graphene substrate. Due to the technical difficulties, 6 nanoplates were measured on the surface of exfoliated graphene.

XRD characterization of the thin films was performed by a Philips X'Pert MRD with a Cu Kα radiation source.

References

1. Kou, L. *et al.* Graphene-based topological insulator with an intrinsic bulk band gap above room temperature. *Nano Lett.* **13**, 6251–6255 (2013).
2. Song, C.-L. *et al.* Topological insulator Bi_2Se_3 thin films grown on double-layer graphene by molecular beam epitaxy. *Appl. Phys. Lett.* **97**, 143118 (2010).
3. Baitimirova, M. *et al.* Vapour-solid synthesis and enhanced thermoelectric properties of non-planar bismuth selenide nanoplates on graphene substrate. *J. Mater. Sci.* **51**, 8224 (2016).
4. Chen, X. *et al.* Flexible bismuth selenide/graphene composite paper for lithium-ion batteries. *Ceramics International* **43**, 1437–1442 (2017).
5. Qiao, H. *et al.* Broadband photodetectors based on graphene–Bi_2Te_3 heterostructure. *ACS Nano* **9**, 1886 (2015).
6. Wyckoff, R. W. G. Crystal structures, 2nd Edition, Krieger: Malabar, FL (1986).
7. Liu, Y., Weinert, M. & Li, L. Spiral growth without dislocations: molecular beam epitaxy of the topological insulator Bi_2Se_3 on epitaxial graphene/SiC(0001). *Phys. Rev. Lett.* **108**, 115501 (2012).
8. Dang, W., Peng, H., Li, H., Wang, P. & Liu, Z. F. Epitaxial heterostructures of ultrathin topological insulator nanoplate and graphene. *Nano Lett.* **10**, 2870–2876 (2010).
9. Kim, N. *et al.* Persistent topological surface state at the interface of Bi_2Se_3 film grown on patterned graphene. *ACS Nano* **8**, 1154–1160 (2014).
10. Ghaemi, P., Mong, R. S. K. & Moore, J. E. In-plane transport and enhanced thermoelectric performance in thin films of the topological insulators Bi_2Te_3 and Bi_2Se_3. *Phys. Rev. Lett.* **105**, 166603 (2010).
11. Jerng, S.-K. *et al.* Ordered growth of topological insulator Bi_2Se_3 thin films on dielectric amorphous SiO_2 by MBE. *Nanoscale* **5**, 10618–10622 (2013).
12. Andzane, J. *et al.* Structure-determined thermoelectric properties of Bi_2Se_3 thin films deposited by vapour-solid technique, in press.
13. Kong, D. *et al.* Few-layer nanoplates of Bi_2Se_3 and Bi_2Te_3 with highly tunable chemical potential. *Nano Lett.* **10**, 2245–2250 (2010).
14. Peng, H. *et al.* Topological insulator nanostructures for near-infrared transparent flexible electrodes. *Nature Chemistry* **4**, 281 (2012).
15. Li, H. *et al.* Controlled synthesis of topological insulator nanoplate arrays on mica. *J. Am. Chem. Soc.* **134**, 6132 (2012).
16. Trivedi, T. *et al.* Versatile large-area custom-feature van der Waals epitaxy of topological insulators. *ACS Nano* **11**, 7457–7467 (2017).
17. Lee, H. C. *et al.* Review of the synthesis, transfer, characterization and growth mechanisms of single and multilayer graphene. *RSC Adv.* **7**, 15644–15693 (2017).
18. Min, Y. *et al.* Solution-based synthesis of anisotropic metal chalcogenide nanocrystals and their applications. *J. Mater. Chem. C* **2**, 6222 (2014).
19. Natl. Bur. Stand. (U.S.) Monogr. **25**, 18 (1981)
20. Zhuang, A. *et al.* Controlling the lateral and vertical dimensions of Bi_2Se_3 nanoplates via seeded growth. *Nano Res.* **8**, 246 (2015).
21. Li, B. *et al.* Strain in epitaxial high-index Bi_2Se_3 (221) films grown by molecular-beam epitaxy. *Appl. Surf. Sci.* **396**, 1825–1830 (2017).
22. Vyshnepolsky, M., Klein, C., Klasing, F., Hanisch-Blicharski, A. & Horn-von Hoegen, M. Epitaxial growth of the topological insulator Bi_2Se_3 on Si(111): growth mode, lattice parameter, and strain state. *Appl. Phys. Lett.* **103**, 111909 (2013).
23. Song, H. S. *et al.* Origin of the relatively low transport mobility of graphene grown through chemical vapour deposition. *Scientific reports* **2**, 337 (2012).

24. Yoon, J.-C., Thiyagarajan, P., Ahn, H.-J. & Jang, J.-H. A case study: effect of defects in CVD-grown graphene on graphene enhanced Raman spectroscopy. *RSC Adv.* **5**, 62772–62777 (2015).
25. Koepke, J. C. *et al.* Atomic-scale evidence for potential barriers and strong carrier scattering at graphene grain boundaries: a scanning tunneling microscopy study. *ACS Nano* **7**, 75 (2013).
26. Moraga, L., Henriquez, R. & Solis, B. Quantum theory of the effect of grain boundaries on the electrical conductivity of thin films and wires. *Physica B* **470–471**, 39–49 (2015).
27. Park, N.-W. *et al.* Effect of grain size on thermal transport in post-annealed antimony telluride thin films. *Nanoscale Res Lett.* **10**, 20 (2015).
28. Chen, J. *et al.* Self healing of defected graphene. *Appl. Phys. Lett.* **102**, 103107 (2013).
29. Lin, Y.-C. *et al.* Graphene annealing: how clean can it be? *Nano Lett.* **12**, 414–419 (2012).
30. Chen, Y. L. *et al.* The annealing effect of chemical vapor deposited graphene IEEE 10th International Conference on ASIC, https://doi.org/10.1109/ASICON.2013.6812069 (2013).
31. Kruskopf, M. *et al.* Epitaxial graphene on SiC: modification of structural and electron transport properties by substrate pretreatment. *J. Phys. Condens. Matter.* **27**, 185303 (2015).
32. Chhikara, M. *et al.* Pentacene on graphene: differences between single layer and bilayer. *Carbon* **69**, 162–168 (2014).
33. Andzane, J. *et al.* Catalyst-free vapour–solid technique for deposition of Bi_2Te_3 and Bi_2Se_3 nanowires/nanobelts with topological insulator properties. *Nanoscale* **7**, 15935 (2015).
34. Kosmaca, J., Andzane, J., Baitimirova, M., Lombardi, F. & Erts, D. Role of nanoelectromechanical switching in the operation of nanostructured Bi_2Se_3 interlayers between conductive electrodes. *ACS Appl. Mater. Interf.* **8**, 12257–12262 (2016).
35. Kunakova, G. *et al.* Bulk-free topological insulator Bi_2Se_3 nanoribbons with magnetotransport signatures of Dirac surface states. *Nanoscale* **10**, 19595–19602 (2018).

Acknowledgements

Author Contributions

J.A. performed the experiments with Bi_2Se_3 deposition on G/SiC, L.B., E.K., A.N. and M.B. performed the experiments with Bi_2Se_3 deposition on CVD graphene and mica and contributed to AFM analysis. S.L.-A. and S.K. prepared G/SiC substrates, contributed to AFM analysis and the manuscript editing. M.B. performed XRD analysis. All authors have contributed to the manuscript writing (with J.A. and D.E. being the main contributors and editors of the manuscript). All authors have given approval to the final version of the manuscript. The datasets generated during and/or analysed during the current study are available from the corresponding author on reasonable request.

Additional Information

Competing Interests: The authors declare no competing interests.

Publisher's note: Springer Nature remains neutral with regard to jurisdictional claims in published maps and institutional affiliations.